Area-averaged evapotranspiration over a heterogeneous land surface: Aggregation of multi-point EC flux measurements with high-resolution land-cover map and footprint analysis

Feinan Xu[1, 2], Weizhen Wang[1], Jiemin Wang[1], Ziwei Xu[3], Yuan Qi[1], Yueru Wu[1]

[1] Key Laboratory of Remote Sensing of Gansu Province, Heihe Remote Sensing Experimental Research Station, Northwest Institute of Eco-Environment and Resources, Chinese Academy of Sciences, Lanzhou, 730000, China
[2] University of Chinese Academy of Sciences, Beijing, 100049, China
[3] State Key Laboratory of Remote Sensing Science, School of Geography, Beijing Normal University, Beijing, 100875, China

Correspondence to: Weizhen Wang (weizhen@lzb.ac.cn)

Abstract. The determination of area-averaged evapotranspiration (ET) at the satellite pixel scale/model grid scale over a heterogeneous land surface plays a significant role in developing and improving the parameterization schemes of the remote sensing based ET estimation models or general hydro-meteorological models. The Heihe Watershed Allied Telemetry Experimental Research (HiWATER) flux matrix provided a unique opportunity to build an aggregation scheme for area-averaged fluxes. Based on HiWATER flux matrix datasets and a high-resolution land cover map derived from aircraft remote sensing, this study focused on estimating the area-averaged ET over a heterogeneous landscape with footprint analysis and multivariate regression. Firstly, the representativeness of multi-point eddy covariance (EC) flux measurements was quantitatively evaluated. Secondly, a flux aggregation method was established combining footprint analysis and multiple regression analysis. The area-averaged sensible heat fluxes were obtained using the method and validated by the large aperture scintillometer (LAS) measurements. Finally, the area-averaged ET of the kernel experimental area of HiWATER was estimated through the established flux aggregation schemes. These findings demonstrate that the refined flux integration technique in this study is a better method to determine the area-averaged fluxes over a heterogeneous suface.

1

1 Introduction

Land surface evapotranspiration (ET) is not only a key component in the regional water circulation, but also essential in the surface energy balances and land surface process. Under the condition of increasing shortage of water resources, high precision estimation of ET at regional scale is essential for those research fields, such as the management of basin water resources, regional planning and the sustainable development of agriculture (Wang et al., 2003). Currently, the commonly used methods for acquisition of regional ET are ground-based observation, remote sensing based estimation and model simulation, respectively.

The Earth's surface is always characterized by spatial heterogeneity, and large land surface heterogeneity affects the exchange of momentum, heat, and water between the land surface and atmosphere (Mengelkamp et al., 2006). Indeed, the surface heterogeneity caused either by the contrast in soil moisture or vegetation type generates a large spatial variability of fluxes which limit the use of the eddy covariance (EC) system, unless one deploys a network of EC devices (Ezzahar et al., 2009b). Flux tower group can quantify the turbulent exchange of energy and mass between the atmosphere and a variety of surface types (Sellers et al., 1995), and these local point measurements need to be aggregated to provide a meaningful area averaged fluxes (André et al., 1986). If special aggregation rules for local flux measurements are applied, measurements can provide averaged fluxes at model grid scale (Beyrich et al., 2006;Mahrt et al., 2001). But given the EC network's high price and the requirement for their continuous maintenance, the large aperture scintillometer (LAS) is a useful alternative method for directly measurements of area-averaged sensible heat fluxes $(1 - 5 \text{ km})$ (Ezzahar et al., 2009b;Ezzahar and Chehbouni, 2009).

Satellite has been considered as a promising data source for deriving regional ET data with the development of remote sensing technique (Ezzahar et al., 2009a). In response to increasing demand for spatially distributed hydrologic information, many satellite-based approaches have been developed for

routine monitoring of ET at regional scale (Anderson et al., 2012). Nevertheless, the effectiveness of the remote sensing based methods for estimating ET must be fully assessed by ground-based area-averaged flux measurements, due to the uncertainties of model inputs and parameterization schemes (Wang et al., 2003). Furthermore, there may be a bias in directly comparing a remote-sensing-based ET estimation with in-situ measurements, because of their spatial-scale mismatch and spatial heterogeneity at the sub-pixel scale (Jia et al., 2012).

General atmospheric-hydrological models (e.g., Numerical Weather Prediction) can adequately describe the interaction between the atmosphere and the underlying surface using complex parameterization schemes. The development and validation of these models are usually based on measurements performed over homogeneous land surfaces. While the assumption of homogeneity might be justified at the local scale (10 m – 10^3 m), it is often violated at the scale of the grid resolution of current regional atmospheric models (about 10^4 m) (Beyrich et al., 2006;Beyrich and Mengelkamp, 2006). Therefore, it is significantly important to determine the area-averaged surface fluxes at the satellite pixel scale/model grid scale (10^3 m – 10^4 m) for the evaluation of general hydro-meteorological models and remote sensing products.

A number of international field experiments have been performed over heterogeneous land surfaces in different geographical and climate regions of the earth in recent decades (Mengelkamp et al., 2006;Beyrich et al., 2006;Wang, 1999), such as HAPEX–MOBILHY (André et al., 1986), FIFE (Sellers et al., 1988), HAPEX-SAHEL (Goutorbe et al., 1994), BOREAS (Sellers et al., 1995), NOPEX (Halldin et al., 1998), LITFASS-2003 (Mengelkamp et al., 2006). In these experiments, based on multi-point flux measurements, surface fluxes at the model grid scale were obtained using various flux aggregation techniques. The aggregated fluxes were also compared with those obtained from LAS systems and remote-sensing estimation methods. The simple flux aggregation methods most commonly used in previous studies mainly include: arithmetic average method, the area-weighted method and the footprint-weighted method (Liu et al., 2016). These studies revealed, the combination of area-averaged

flux measurements and multi-site flux measurements with simple flux aggregation schemes can provide reasonable estimates over a heterogeneous land surface (Mahrt et al., 2001;Beyrich et al., 2006;Liu et al., 2016).

However, the integration schemes of aforementioned methods are applicable for relative uniform sites, the local flux measurements of which are representative of the individual surface type. For the interpretation of tower flux measurements over a heterogeneous land surface, footprint analysis can be an operational approach (Schmid, 2002). The development of footprint models provides diagnostic tools to quantify the representative of tower flux measurements for selected sites (Horst and Weil, 1992;Kim et al., 2006). Besides, it had been demonstrated that the footprint climatology can be combined with information on the spatial variability of vegetation types provided by satellite image (Kim et al., 2006;Chen et al., 2008). Land cover reflects the combined effects of vegetation, climate, soil and topography, some relationship should be expected between land cover and measured surface fluxes (Ogunjemiyo et al., 2003). Ran et al. (2016) proposed four indicators with footprint analysis and land-cover type map to improve the representative of EC towers and correct the EC flux measurements. But this method didn't obtain the surface fluxes of individual land cover types but just corrected the EC observations with some prior coefficients. Some previous studies have successfully related the aircraft observed fluxes to surface cover types with the combination of footprint models and remotely sensed land classification map (Ogunjemiyo et al., 2003;Kirby et al., 2008;Hutjes et al., 2010). Among these work, a flux dis-aggregation method (Hutjes et al., 2010), developed from former study presented by Ogunjemiyo et al. (2003), would be a promising method for integrate multiple tower-based flux measurements to satellite pixel or grid scale on account of its theoretical framework. The application of this method in attributing heterogeneous EC flux measurements to separate land over classes would be a hopeful way to have insight into the component fluxes over a heterogeneous surface, and develop a flux aggregation scheme to explore the use of multi-point EC flux measurements for the estimation of the area-averaged surface fluxes.

A multi-scale observation experiment on evapotranspiration over a heterogeneous land surface was conducted in the middle reaches of Heihe River Basin during the HiWATER (Heihe Watershed Allied Telemetry Experimental Research) program in 2012 (Li et al., 2013;Liu et al., 2016). A comprehensive flux matrix, consisted of 18 EC systems and four groups of LAS systems within a 5×5 km^2 area, was specifically designed to capture the multi-scale characteristics of ET over a heterogeneous landscape during the experiment. HiWATER flux matrix, with an abundant of multi-scale flux measurements, provided a unique opportunity to build an aggregation scheme for area-averaged fluxes over a heterogeneous land surface. The objective of this study was to integrate multi-point EC flux measurements to area-averaged fluxes over a heterogeneous land surface with high resolution land-cover data and footprint analysis. The main issues were as followed: (1) the representative of EC flux matrix was quantitatively evaluated; (2) a flux aggregation scheme was established to estimate area-averaged sensible heat fluxes, taking LAS measurements as reference; (3) the developed flux aggregation method was used to determine the area-averaged evapotranspiration.

2 Study sites and data

2.1 Site description

This study was based on ground-based observation datasets, collected from the multi-scale flux matrix of HiWATER program from May to September 2012. The kernel experimental area (5×5 km^2) of the multi-scale observation experiment was located in the Yingke and Daman irrigation district within Zhangye oasis. The land-cover types were dominated by maize (72 %), vegetables (5 %), orchard and shelterbelt (8 %), residential area and roads (15 %). As shown by the numbers 1 − 17 in the following Fig. 1, 17 sites were installed according to the distribution of crop planting structure and land cover. Each of them was equipped with an eddy covariance system (with two layers in site 15) and an automatic weather station (AWS), to capture the exchange process of surface water and energy budget at the local scale and micrometeorological elements near the surface layer. Spatial distribution of

EC/AWS systems is shown in Fig. 1, with site 1 of vegetable (pepper) field, site 4 of residential area, site 17 of apple orchard, and the others are in maize fields. Key micrometeorological measurements observed at each AWS included four-component radiation, one or two levels wind / temperature / relative humidity profile, soil temperature / moisture and soil heat flux, etc. Among these sites, site 15 was a superstation equipped with two levels EC system, and seven-level wind speed/direction, air temperature/humidity profiles. 4 paths of large aperture scintillometer devices were installed crossed over the experimental district to obtain area-averaged sensible heat fluxes (see Fig. 1). Details of the EC and LAS systems in the flux matrix were given in Table 1 and Table 2, respectively.

2.2 Data collection and processing

2.2.1 Flux data processing

Data in typical clear days of 29 to 30 June 2012 were selected for the following analysis, including EC data from 16 towers (except site 3 and highest level (34 m) of site 15) and LAS data as well as multi-point micrometeorological data list above. The last round of irrigation in each plot was done before 26 June. During the two days, there was almost no irrigation in the flux matrix. At first, AWS data sampled at 10 min were averaged to 30 min period. Secondly, careful data processing and quality control for EC and LAS raw data were performed to obtain high quality flux data.

The EddyPro software (www.licor.com/eddypro) developed by the American LI-COR company was used to process and calculate the 10 Hz raw EC data into a half-hour averaged flux data by several procedures, including spike removal, angle of of attack correction (for Gill), time lag correction, coordinate rotation (2-D rotation), frequency response correction, sonic virtual temperature correction, and corrections for density fluctuation (Webb-Pearman-Leuning, WPL). Data quality assessment was performed for the turbulent flux in each 30 min using the flag system (0, 1 and 2) (Mauder and Foken, 2004). Detailed information on the processing steps of EC raw data can be found in Wang et al. (2015) and Xu et al. (2013).

The flux data of flag 2 were discarded, as well as the data at night when the friction velocity was below 0.1 m s^{-1} (Blanken, 1998; Liu et al., 2011). To obtain daily ET, a gap-filling method based on the nonlinear regression (establishing the relationship between the latent heat flux and the net radiation) was used to fill the gaps between the 30 min latent heat flux data. Finally, the daily ET was calculated by summing the half-hourly gap-filled ET to 24 h totals.

The LAS system provided a measurement of the structure parameter for the refractive index of air (C_n^2) with an output period of 1 min, the raw LAS data were, firstly, averaged to 30 min (the LAS data only observed by the BLS series were collected). Then, the path-average sensible heat fluxes were iteratively calculated combining EC data (e.g. length of stability and Bowen ratio) and meteorological data (e.g. wind speed, air temperature, pressure) based on Moninin—Obukhov Similarity Theory (MOST) (Andreas, 1988). And the inputs of the roughness height and zero-plane displacement were obtained following Martano (2000). To perform the quality control for raw LAS data, the equation $C_n^2 < 0.193L_{LAS}{}^{8/3}\lambda^{1/3}D^{5/3}$ (L_{LAS} is the path length, D is the diameter of optical aperture, and λ is wavelength) was applied to reject the data whose value exceeded the saturated criterion (Ochs and Wilson, 1993). Only sensible heat fluxes from LAS measurements for daytime (8:30 am − 15:30 pm, Beijing Standard Time, BST; the time difference between Local time and BST is approximately +1 h 18 min) were selected in this study.

For the ECs used in our data analysis, the systematic errors had been tried to reduce to a minimum with a pre-observation intercomparison (Xu et al., 2013) and careful maintenance during the observation. The random errors were also analyzed by a separate research (Wang et al., 2015), which can be minimized in an ensemble average. As for the LASs, the errors from data processing processes (e.g. the Bowen-ratio correction problem) were also tried to minimize as much as possible through intercomparisons with fluxes from EC.

For the ECs, the energy balance closure ratio (EBR) was also assessed (Xu et al., 2017). The ratio

of the turbulent heat flux (the sensible and latent heat flux) to available energy for 16 EC sites over vegetated surfaces was 87 %, and the EBR for site 4 was 0.84.

2.2.2 Collection and processing of remote-sensing data products

A land cover classification map with 1-m spatial resolution was collected. The map was derived from the airborne hyper-spectral images acquired by the Compact Airborne Spectrographic Imager (CASI) on 29 June 2012 and the Canopy Height Model (CHM) data from the LiDAR data collected on 9 July 2012 using an object-based classification method. The classification accuracy of the 1-m land cover map is up to 90 %, and Kappa coefficient is approximately 0.9. The detailed classification process of the map can be found in Liu and Bo (2015).

However, there still occurred land cover misclassification in the collected map, despite high accuracy of the land cover product. One of the reasons is the spectral similarity between different surface cover types. To obtain a much more accurate land cover map, the misclassified patches of land cover in the kernel experimental area were visually and manually revised based on high-resolution CCD images acquired on 26 July and Google Earth imagery on 3 September 2012. Finally, for the aim of this study, the refined 12 kinds of land classification types in the study area were merged into four kinds (maize, vegetables, woods and non-vegetation types) according to crop species and surface types. As shown in Fig. 1, among the four land types, non-vegetation types mainly contain two types of land surface cover, namely buildings and road.

3 Methodology

3.1 Aggregation method combining footprint analysis and multivariate regression

It is general accepted that an average flux equals the area-weighted sum of the component fluxes emanating from individual land cover classes (Hutjes et al., 2010).

$$F = \sum_{k=1}^{n} A_k F_k \tag{1}$$

Where F is the total flux of any scalar (here the heat and water vapor flux are on the study) for a specified area, A_k is the fractional coverage of an individual land cover class k within that area, and F_k is the flux emanating from that individual land cover class, n is the number of land cover classes that is distinguished in the specified area.

Then, the observed flux (F_{obs}) at height z_m can be closely related to the true surface flux upwind of measurement point through the footprint function, in continuous form (Leclerc and Foken, 2014):

$$F_{obs}(x_{obs}, y_{obs}, z_m) = \int_{-\infty}^{\infty} \int_{-\infty}^{\infty} F(x, y, 0) w(x, y, z_m) dx dy \tag{2}$$

Here x_{obs}, y_{obs} are the site coordinates, z_m is the effective observation height defined as $z_m = z - d$, z is the sensor height, d is the zero plane displacement. The footprint function $w(x, y, z_m)$ describes the flux portion seen at (x_{obs}, y_{obs}, z). Equation (2) can be discretized for a uniform grid over a landscape, as in a remote-sensing image based land-cover map, leaving out the height dependence for simplification. Equation (2) becomes:

$$F_{obs} = \sum_{k=1}^{n} F_k \sum_{i=1}^{N} \sum_{j=1}^{M} w_{ij} \Delta x \Delta y \tag{3}$$

Where each pixel $\Delta x \Delta y$ of the map is assumed to be homogeneous, which is uniquely classified as belonging to class k. Then the fraction X of the k-th land cover type in the footprint (fp) was defined as:

$$X_{fp,k} = \sum_{i=1}^{N} \sum_{j=1}^{M} w_{ij} \Delta x \Delta y \tag{4}$$

Combing the Eq. (3) and Eq. (4), the multi-linear model for the flux becomes:

$$F_{obs} = \sum_{k=1}^{n} F_k X_{fp,k} \tag{5}$$

A critical assumption under the flux aggregation method is that each land cover k (area A_k) is with a

9

constant source strength (F_k). Then Flux F for a specific area is a weighted aggregation of its various land cover classes. Base on multi-point tower flux measurements, multi-linear regression equations can be formulated by overlaying the flux footprint with high resolution land cover map (Eq. 5). The equations could be solvable to get F_k with the Least Squares method, when the number of flux towers is greater than that of land cover classes (n). For each LAS path, the observed (sensible heat) flux can be dis-aggregated by relevant footprint function as Eq. (5). This can be taken as a validation of the former step.

The accuracy of this aggregation technique is highly dependent on four aspects: (1) better flux data for all EC sites; (2) better land cover classification map; (3) more precise flux footprint analysis; (4) good flux and footprint data for LAS. So properly processed flux data, accurate high-resolution land cover map and appropriate footprint functions are the fundamental of formulating a better multiple linear regression. Sometimes, the established multi-linear regression equations may not be solvable because of the improper adoption of low-accuracy land cover classification map or imperfectly known footprint model. When suffered this problem, the classification accuracy of the used land cover map should be checked, and the selected footprint model should be verified whether it's applicable.

3.2 Footprint models

The Eulerian analytical footprint model, which developed by Kormann and Meixner (2001), was used to estimate the single time flux footprint of EC measurements, due to its ease of use and wide range of stability as well as its numerical stability (Leclerc and Foken, 2014). This footprint function $w(x, y, z)$ can be expressed in terms of a crosswind integrated flux footprint function, $f^y(x, z)$, and a Gaussian crosswind distribution function, $D_y(x, y)$. The footprint function equation is followed by Eq. (6). More details on the mentioned parameters can be seen in Kormann and Meixner (2001).

$$w(x, y, z) = f^y(x, z) \bullet D_y = \frac{1}{\Gamma(\mu)} \frac{\xi^\mu}{x^{1+\mu}} e^{-\xi/\mu} \bullet \frac{1}{\sqrt{2\pi}\sigma} e^{-\frac{y^2}{2\sigma^2}} \qquad (6)$$

The flux contribution source area of the LAS measurements can be assessed by combining the footprint model for point measurement with the path-weighting function $W(x)$ of the LAS (Meijninger et al., 2002). For equal sized transmitter and receiver apertures, this path-weighting function is symmetrical bell-shaped having a center maximum and tapering to zero at the transmitter and receiver end. The equation of footprint function of LAS is that:

$$f_{LAS} = \int_{x_2}^{x_1} W(x) \bullet w(x - x', y - y', z_{LAS}) dx \tag{7}$$

Where x_1, x_2 are the positions of the LAS receiver and transmitter, respectively. x, y represent the locations of points along the optical path length of the LAS. x', y' are the coordinates upwind of each of the points. z_{LAS} is the effective height of the LAS measurements.

To obtain the daily flux footprint of the EC flux measurements, the flux-weighted footprint climatology method was applied for each pixel (Liu et al., 2016). The expression of the weighted footprint climatology is shown in Eq. (8).

$$w_c(x, y, z) = \sum_i^N w_i(x, y, z) \bullet Flux(i) \Big/ \sum_i^N Flux(i) \tag{8}$$

Here i denotes the timestep (e.g. 30 min), N is the total number of 30-min periods within the time frame (e.g. daily), $Flux(i)$ is the observed flux at i time-step (e.g. ET for every 30-min in this study), $w_i(x, y, z)$ represents every half-hourly footprint calculated by Eq. (6).

The inputs of the footprint models mainly include the measurement height, wind direction, wind speed and the Obukhov length. The values of these input parameters can be derived from measurements generally available from EC flux towers. The daily flux contribution area of the EC flux measurements was calculated by Eq. (8), which provides approximately 90 % of the total source area that contributes to the measured fluxes. Every 30-min flux source area of the LAS sites was estimated via Eq. (7), and the 90 % half-hourly footprint contours of LAS measurements were used. The normalized daily footprint climatology of ECs and half-hourly footprint estimates of LASs were individually overlaid

11

with 1-m land cover map to determine the footprint-weighted contribution of each land cover classes to the measured flux from EC and LAS systems.

3.3 Data processing flow of the determination of area-averaged fluxes

The overall data processing flow for determining the area-averaged evapotranspiration over a heterogeneous land surface mainly includes three aspects (Fig. 2).

Firstly, the spatial representativeness of the 16 EC flux towers within the 5×5 km^2 experiment area was quantitatively assessed by overlaying in-site flux footprint climatology with 1-m land cover map. Detailed analyses on this aspect are going to be presented in the following section.

The second aspect was to evaluate the reliability of the established flux aggregation schemes. The land cover specific flux was firstly dis-aggregated from multiple EC flux measurements by performing a multiple linear regression analysis (Eq. 5). The EC dis-aggregated fluxes of each land cover classes were then aggregated again to obtain area-averaged fluxes, according to the fractional weight of each land cover class in the LAS footprint (Eq. 4). Finally, the aggregated fluxes were compared with LAS observations.

At last, the area-averaged evapotranspiration over a heterogeneous land surface was estimated from multi-point EC flux measurements with the developed flux integration schemes, based on footprint analysis and high resolution land cover map.

4 Results and Discussion

4.1 The characteristics of the surface heat and water vapor fluxes

Figure 3 depicts the diurnal cycle of the sensible (Fig. 3a) and latent (Fig. 3b) heat fluxes at different sites on two clear days. Both of the two figures reveal significant differences in the magnitude of the sensible- and latent heat fluxes between different surface types during the growing season.

The sensible heat flux over residential area reached a maximum of about 150 W m^{-2} at afternoon

and was higher than that over the vegetated surfaces (H_ec4, Fig. 3a), while the latent heat flux was smaller compared with other sites, with maximum value of less than 300 W m^{-2} due to a certain fraction of sealed land surfaces (LE_ec4, Fig. 3b).

Over the vegetated surfaces (orchard, vegetable, maize), the sensible heat flux was nearly less than 100 W m^{-2} because of well-irrigated cropland (Fig. 3a). The sensible heat flux over the three types of vegetation was also significantly different, and there was also a difference in sensible heat fluxes among maize sites. The mean value of the standard deviation (SD) of H for 13 maize sites was about 8.4 W m^{-2} (Fig. 4a).

Deviations in latent heat fluxes over different vegetation types were also found (Fig. 3b, Fig. 4b). The maize fields performed highly latent heat fluxes and lower sensible heat fluxes than the other two vegetated surfaces. One of the possible reasons is that both of the orchard area and the vegetable field are relatively sparse compared with the maize cropland.

The mean value of the SD of LE for all maize sites was approximately 43.3 W m^{-2}. The result showed that the latent heat flux over maize cropland exhibited larger SD than the sensible heat flux, and it also indicated the LE differed between sites for same underlying surface (Fig. 4). This can be partly explained by the discrepancy in plant physiology and vegetation growing stage.

The preliminary results indicated that the variability and difference in the surface energy fluxes between the HiWATER tower flux sites was significant during the crop growth period. The differences in sensible and latent heat fluxes between maize field sites also could be noticed.

4.2 Analysis of the representativeness of the multi-point EC flux measurements

To further understand the variability of surface energy fluxes between different sites in a heterogeneous landscape, the footprint analyses for representativeness of EC sites were applied by overlaying flux footprint with high resolution land-cover map (Fig. 1). The fraction of land cover classes present in the daily-averaged footprint of each EC measurements is given in Fig. 5. Given the

source area (90 % flux contribution) of the 4 ECs (sites 5, 8, 13 and 16) on 30 June 2012 exceeded the extent of land cover map, the spatial representative of the 4 EC sites were not shown in Fig. 5b.

Due to the variations in the observation height, atmospheric stability, wind direction and wind speed, the exact shape and size of the EC source area were distinctly different (Fig. 1). For each EC flux measurements, there was more than one type of land cover in its footprint. The contribution of each land cover classes to the total measured flux for EC sites was changed with the varying source area (Fig. 5).

The dominated surface types in the source area were vegetable and orchard at sites 1 and 17, respectively. For site 4, however, there were mainly three types of land cover within its footprint, namely non-vegetation, maize and woods type. The fractional weight of the non-vegetation type and maize field in the footprint greatly varied, while the proportion of woods was almost changeless.

At maize field sites, the relative contribution of maize field to the EC measured flux was approximately more than 0.9, except for sites 2, 9 and 10. At site 2, the percentage of non-vegetation type in the footprint was almost 0.18. For site 9, the rate of maize and non-vegetation type present in footprint significantly varied. The contribution of vegetable type to the flux measurements at site 10 ranged from 0.15 to 0.1.

The above analysis shows that the tower flux measurements at the field scale are generally representative of multiple surface types. The result indicates that the latent and sensible heat fluxes measured by EC systems are representative of the averaged fluxes, which are weighted the upwind surface flux emanating from individual land cover classes with flux footprint. In general, it may be problematic to validate the model estimated fluxes by direct comparison with tower-based flux measurements over a heterogeneous land surface. Thus, the extension of multiple flux measurements to pixel/grid scale surface fluxes is urgently needed.

4.3 Evaluation of the EC aggregated fluxes

The determination of area-averaged fluxes from point measurements is usually not straightforward,

14

especially for heterogeneous land surfaces. Based on multi-point EC flux measurements and accurate 1-m land cover map, a flux aggregation method was established to estimate averaged surface fluxes with footprint analysis and multivariate regression. Fig. 1 shows that all types of land covers present in the LAS flux footprint, so the LAS measurements can be taken as reference to assess the feasibility of the developed integration schemes.

At first, the sensible heat flux for each land cover was dis-aggregated from the EC observed component fluxes in a heterogeneous footprint with multiple linear regression method. The diurnal cycle of the EC dis-aggregated sensible heat fluxes for each land cover types is highly significant (Fig. 6). During the crop growth stage, the sensible heat flux over maize field showed a minimum value in the afternoon, while the sensible heat fluxes for non-vegetation type at daytime exhibited a maximum of about 200 W m^{-2}. The sensible heat fluxes for vegetable and woods types lied between them.

Then, the sensible heat flux representative for the LAS source area was aggregated by multiplying the EC dis-aggregated fluxes for the four land-cover classes by their relative fraction in the LAS source area. Fig. 7 illustrates a scatterplot of 30-min averaged sensible heat fluxes estimated using the flux aggregation method (hereafter referred as H_ECagg) versus LAS measurements (H_LAS), as well as the linear regression parameters (including equations and R^2). The different statistics between LAS observed fluxes and EC aggregated results are listed in Table 3.

For LAS 1 (see Fig. 7a and Table 3), a good agreement is found between EC aggregated fluxes and LAS measurements, with high correlation coefficient and low RMSE value (R^2= 0.79, RMSE= 0.96 W m^{-2}). The scatter points in the graph are nearly close to the 1:1 line. The MBE and MAPE values were 4.25 W m^{-2} and 9.93 %, respectively.

Compared with LAS 1, there was a little scatter between LAS measured fluxes and estimates from multiple EC flux observations for LAS 2, but yielding a small mean bias error (MBE = 2.31 W m^{-2}) (Fig. 7b, Table 3). RMSE and MAPE values between H_ECagg and H_LAS2 were much higher than that of LAS 1, with values of 6.91 W m^{-2} and 16.39 %, respectively. Considering the heterogeneous

15

distribution of surface covers in the LAS source area, slight area of non-vegetation distributing in the center of LAS 2 path would be the primary factor attributing to the bias (blue circles in Fig. 1).

For LAS 3 (Fig. 7c, Table 3), there was a slightly weak relationship between sensible heat fluxes derived from the LAS measurements and flux aggregation method, with correlation coefficient (R^2) of 0.57 and RMSE, MAPE and MBE values of 17.63 W m^{-2}, 31.7 % and -18.01 W m^{-2}, respectively. The scatter points in Fig. 7c were overall below the 1:1 line. It indicated that the 30-min averaged H estimated from EC flux observations using the aggregation method were underestimated against LAS derived H (negative MBE). As shown in Fig. 1, there is more large area of residential areas randomly distributing in the center of LAS 3 path than other three LAS systems. This discrepancy is likely related to the heterogeneously distributed surface types.

In Fig. 7d, the area-averaged sensible heat fluxes obtained using the flux aggregation method were consistent with LAS measurements, with R^2 of 0.57 for LAS 4. In contrast with LAS 3, the scatter points in this graph were almost above the 1:1 line (overestimate of EC estimated H, MBE > 10 W m^{-2}). RMSE value of LAS 4 relatively decreased by 4.88 W m^{-2}, but MAPE value was up to 33.7 %. The red open squares in Fig. 7d are more close to the 1:1 line than the blue open circles. When southeast wind prevailed, the relative contribution of non-vegetation type to the LAS 4 measurements was about 0.2, and its value decreased to 0.08 when the main wind direction was northwest.

Through detailed analysis, the magnitude of divergences between the estimated and measured area-averaged surface fluxes is in large part concerned with the variation of corresponding LAS source area. Moreover, the contribution of non-vegetation type to the LAS observations, which accounted for a large proportion in the footprint of LASs (LAS 2, 3 and 4), would be one of the main factors contributing to the bias between the estimated results and LAS measurements. The reason is that the EC dis-aggregated sensible heat flux for non-vegetation type may not be representative for the flux emanating from sealed buildings and roads that are part of non-vegetation type. On the other hand, the complexity of the LAS footprints may lead to the inconsistency of EC-estimated and LAS-measured

averaged fluxes.

Overall, the above results demonstrate that, compared with the area-averaged fluxes measured by LAS systems, the area-averaged fluxes that are aggregated from multiple EC flux measurements using the established flux aggregation method are reliable. Therefore, the developed flux integration schemes in this study can be an effective way to estimate areal averaged fluxes.

4.4 Estimation of area-averaged evapotranspiration

The flux aggregation scheme, which was established and evaluated in Sect. 4.3, was adopted to determine the area-averaged ET over our study area with multi-point EC flux measurements and high resolution land-cover map. The EC dis-aggregated daily ET for all the land covers over two clear days was shown in Fig. 8. As can be seen, the daily ET values for maize field were highest during the crop growing season (7 mm – 8 mm). The value of daily ET was 6.4 mm for woods type, and it ranged from 6 mm to 7 mm for vegetable type. On the contrary, the daily ET for non-vegetation type varied largely, with values of 2.8 mm on 29 June and 1.5 mm on 30 June, respectively.

The daily ET maps at 1-m resolution were produced through the dis-aggregated daily ET for all land cover classes, combined with the 1-m land classification map. Fig. 9 depicts the spatial pattern of daily ET on 29 and 30 June 2012. It can be seen from the legend in figure, the daily ET ranged from 1.56 to 7.95 mm during the two days, and with higher values on 29 June (Fig. 9a) for all land cover classes than that on 30 June (Fig. 9b). The maize field performed highest ET value and distributed widely, whereas other three types of land cover randomly distributed across the whole study area with quite different ET values.

Table 4 lists the total ET for different land cover classes and their proportion of the total area ET. The total ET for our study area was almost 169626.77 m^3 on 29 June, while it was about 152948.41 m^3 on 30 June. The results demonstrated that the ratio of ET for maize field to the total area ET was in excess of 80 %. In addition, the total rate of ET for both woods and vegetables types was approximately

17

13 %, and the ET value for non-vegetation type accounted for 4.83 % of daily totals on the average.

Finally, the area-averaged daily ET over the kernel experiment area of HiWATER was estimated via Eq. (1), with values of approximately 7.01 mm on 29 June and 6.32 mm on 30 June 2012.

5 Summary and conclusions

On the basis of 1-m accurate land cover map and multi-point ground-based flux measurements datasets from 16 EC systems and 4 groups of LAS systems during the intensive observation period of HiWATER program, the area-averaged surface fluxes over a heterogeneous surface were determined by a flux aggregation method, which was established through the integration of footprint analysis and multiple regression. The estimated area-averaged fluxes were validated by the LAS measurements to assess the reliability of the integration method. Ultimately, the method that had been evaluated was used to estimate area-averaged ET over our study area.

First and foremost, analyses of the spatial representativeness of multiple EC flux towers were performed for the interpretation of the surface fluxes over different land surfaces. It is proved that the combination of footprint analysis and high-resolution land cover map can be a proper way to clarify the relationship between the tower-based flux observations over heterogeneous surfaces and individual land cover specific fluxes, and it is also the foundation for the establishment of flux aggregation scheme.

Secondly, based on good multi-scale (EC & LAS) flux datasets, precise flux footprints of flux towers and better land cover classification map, a flux aggregation scheme can be successfully established through the integration of footprint analysis and multivariate regression. In a heterogeneous study area, the surface flux emanating from individual land cover classes need to be firstly acquired by a flux integration method before deriving area-averaged fluxes. The results show that the developed flux aggregation method provides a unique opportunity to disentangle the heterogeneous land surface fluxes in their single components.

Then, the averaged surface fluxes estimated from the established flux aggregation method were

compared with the corresponding observed LAS values. The MAPE values of the LAS 1, LAS 2, LAS 3 and LAS 4 were 9.93 %, 16.39 %, 31.7 % and 33.7 %, respectively. The reasons for the divergences between EC aggregated estimates and LAS observations were investigated by a combination of remote sensing data and ground measurements, and the findings revealed that the extent of vegetation structure heterogeneity had a significant influence on the application of the established aggregation method.

In spite of the limitations mentioned above, the flux integration technique refined in this study is feasible for the estimation of area-averaged fluxes over a heterogeneous land surface. Besides, with abundant flux matrix datasets and high accuracy land cover map, the refined method can achieve the goal of determining the area-averaged ET over an irrigated cropland district.

The results of this study also suggest, the dis-aggregation process that attribute EC observed fluxes over heterogeneous land surface to separate land cover classes has the potential to scale up multiple EC measurements to an oasis landscape, even to a whole river basin through further studies, especially evapotranspiration. The implication of this result is not only greatly important for improving the parameterization schemes of surface fluxes in meso-scale (1 ~20 km) models but quite interested for hydrological modeling and basin water resource management.

Data availability

The flux observation matrix datasets from the eddy covariance (EC) systems and large aperture scintillometer (LAS) systems and the meteorological data in this study are available at http://card.westgis.ac.cn/hiwater/mso on request. The revised 1-m land cover data for this paper are available from the corresponding author on request.

Competing interests

The authors declare that they have no conflict of interest.

References

Anderson, M. C., Kustas, W. P., Alfieri, J. G., Gao, F., Hain, C., Prueger, J. H., Evett, S., Colaizzi, P., Howell, T., and Chávez, J. L.: Mapping daily evapotranspiration at Landsat spatial scales during the BEAREX'08 field campaign, Advances in Water Resources, 50, 162-177, 2012.

André, J.-C., Goutorbe, J.-P., and Perrier, A.: HAPEX-MOBLIHY: A Hydrologic Atmospheric Experiment for the Study of Water Budget and Evaporation Flux at the Climatic Scale, Bulletin of the American Meteorological Society, 67, 138-144, 1986.

Andreas, E. L.: Estimating Cn^2 over snow and sea ice from meteorological data, JOSA A, 5, 481-495, 1988.

Beyrich, F., Leps, J.-P., Mauder, M., Bange, J., Foken, T., Huneke, S., Lohse, H., Lüdi, A., Meijninger, W. M., and Mironov, D.: Area-averaged surface fluxes over the LITFASS region based on eddy-covariance measurements, Boundary-layer meteorology, 121, 33-65, 2006.

Beyrich, F., and Mengelkamp, H.-T.: Evaporation over a heterogeneous land surface: EVA_GRIPS and the LITFASS-2003 experiment—an overview, Boundary-layer meteorology, 121, 5-32, 2006.

Blanken, P.: Turbulent flux measurements above and below the overstory of a boreal aspen forest, Boundary-Layer Meteorology, 89, 109-140, 1998.

Chen, B., Black, T. A., Coops, N. C., Hilker, T., Trofymow, J. A., and Morgenstern, K.: Assessing Tower Flux Footprint Climatology and Scaling Between Remotely Sensed and Eddy Covariance Measurements, Boundary-Layer Meteorology, 130, 137-167, 10.1007/s10546-008-9339-1, 2008.

Ezzahar, J., and Chehbouni, A.: The use of scintillometry for validating aggregation schemes over heterogeneous grids, Agric. For. Meteorol., 149, 2098-2109, 2009.

Ezzahar, J., Chehbouni, A., Er-Raki, S., and Hanich, L.: Combining a large aperture scintillometer and estimates of available energy to derive evapotranspiration over several agricultural fields in a semi-arid region, Plant Biosystems - An International Journal Dealing with all Aspects of Plant Biology, 143, 209-221, 10.1080/11263500802710036, 2009a.

Ezzahar, J., Chehbouni, A., Hoedjes, J., Ramier, D., Boulain, N., Boubkraoui, S., Cappelaere, B., Descroix, L., Mougenot, B., and Timouk, F.: Combining scintillometer measurements and an aggregation scheme to estimate area-averaged latent heat flux during the AMMA experiment, Journal of hydrology, 375, 217-226, 2009b.

Goutorbe, J., Lebel, T., Tinga, A., Bessemoulin, P., Brouwer, J., Dolman, A., Engman, E., Gash, J., Hoepffner, M., and Kabat, P.: HAPEX-Sahel: a large-scale study of land-atmosphere interactions in the semi-arid tropics, Annales Geophysicae, 12, 53-64, 1994.

Halldin, S., Gottschalk, L., van de Griend, A. A., Gryning, S.-E., Heikinheimo, M., Högström, U., Jochum, A., and Lundin, L.-C.: NOPEX—a northern hemisphere climate processes land surface experiment, Journal of Hydrology, 212, 172-187, 1998.

Horst, T., and Weil, J.: Footprint estimation for scalar flux measurements in the atmospheric surface layer, Boundary-Layer

Meteorology, 59, 279-296, 1992.

Hutjes, R., Vellinga, O., Gioli, B., and Miglietta, F.: Dis-aggregation of airborne flux measurements using footprint analysis, Agric. For. Meteorol., 150, 966-983, 2010.

Jia, Z., Liu, S., Xu, Z., Chen, Y., and Zhu, M.: Validation of remotely sensed evapotranspiration over the Hai River Basin, China, Journal of Geophysical Research: Atmospheres, 117, http://dx.doi.org/10.1029/2011jd017037., 2012.

Kim, J., Guo, Q., Baldocchi, D., Leclerc, M., Xu, L., and Schmid, H.: Upscaling fluxes from tower to landscape: Overlaying flux footprints on high-resolution (IKONOS) images of vegetation cover, Agric. For. Meteorol., 136, 132-146, 10.1016/j.agrformet.2004.11.015, 2006.

Kirby, S., Dobosy, R., Williamson, D., and Dumas, E.: An aircraft-based data analysis method for discerning individual fluxes in a heterogeneous agricultural landscape, Agric. For. Meteorol., 148, 481-489, 2008.

Kormann, R., and Meixner, F. X.: An analytical footprint model for non-neutral stratification, Boundary-Layer Meteorology, 99, 207-224, 2001.

Leclerc, M. Y., and Foken, T.: Footprints in Micrometeorology and Ecology, Springer, Heidelberg, New York, Dordrecht, London, XIX, 239 pp., 2014.

Li, X., Cheng, G., Liu, S., Xiao, Q., Ma, M., Jin, R., Che, T., Liu, Q., Wang, W., Qi, Y., Wen, J., Li, H., Zhu, G., Guo, J., Ran, Y., Wang, S., Zhu, Z., Zhou, J., Hu, X., and Xu, Z.: Heihe Watershed Allied Telemetry Experimental Research (HiWATER): Scientific Objectives and Experimental Design, Bulletin of the American Meteorological Society, 94, 1145-1160, 10.1175/bams-d-12-00154.1, 2013.

Liu, S., Xu, Z., Wang, W., Jia, Z., Zhu, M., Bai, J., and Wang, J.: A comparison of eddy-covariance and large aperture scintillometer measurements with respect to the energy balance closure problem, Hydrology & Earth System Sciences, 15, 1291-1306, 2011.

Liu, S., Xu, Z., Song, L., Zhao, Q., Ge, Y., Xu, T., Ma, Y., Zhu, Z., Jia, Z., and Zhang, F.: Upscaling evapotranspiration measurements from multi-site to the satellite pixel scale over heterogeneous land surfaces, Agric. For. Meteorol., 230, 97-113 2016.

Liu, X., and Bo, Y.: Object-Based Crop Species Classification Based on the Combination of Airborne Hyperspectral Images and LiDAR Data, Remote Sens., 7, 922-950, 2015.

Mahrt, L., Vickers, D., Sun, J., and McCaughey, J. H.: Calculation of area-averaged fluxes: Application to BOREAS, Journal of applied meteorology, 40, 915-920, 2001.

Martano, P.: Estimation of surface roughness length and displacement height from single-level sonic anemometer data, Journal of Applied Meteorology, 39, 708-715, 2000.

Mauder, M., and Foken, T.: Documentation and instruction manual of the eddy covariance software package TK2. Department of Micrometeorology, University of Bayreuth Rep. 26, 44 pp, 2004.

Meijninger, W., Hartogensis, O., Kohsiek, W., Hoedjes, J., Zuurbier, R., and De Bruin, H.: Determination of area-averaged sensible heat fluxes with a large aperture scintillometer over a heterogeneous surface–Flevoland field experiment, Boundary-Layer Meteorology, 105, 37-62, 2002.

Mengelkamp, H.-T., Beyrich, F., Heinemann, G., and Ament, F., Bange, J., Berger, F. H., Bösenberg, J., Foken, T., Hennemuth, B., Heret, C., Huneke, S., Johnsen, K.-P., Kerschgens, M., Kohsiek, W., Leps, J.-P., Liebethal, C., Lohse, H.,

21

Mauder, M., Meijninger, W. M. L., Raasch, S., Simmer, C., Spieß, T., Tittebrand, A., Uhlenbrook, S., and Zittel,P.: Evaporation over a heterogeneous land surface: the EVA-GRIPS project, Bulletin of the American Meteorological Society, 87, 775-786, 2006.

Ochs, G., and Wilson, J.: A Second-generation Large-aperature Scintillometer, US Department of Commerce, National Oceanic and Atmospheric Administration, Environmental Research Laboratories, Wave Propagation Laboratory, 1993.

Ogunjemiyo, S. O., Kaharabata, S. K., Schuepp, P. H., MacPherson, I. J., Desjardins, R. L., and Roberts, D. A.: Methods of estimating CO_2, latent heat and sensible heat fluxes from estimates of land cover fractions in the flux footprint, Agric. For. Meteorol., 117, 125-144, 2003.

Qiao, C., Sun, R., Xu, Z., Zhang, L., Liu, L., Hao, L., and Jiang, G.: A Study of Shelterbelt Transpiration and Cropland Evapotranspiration in an Irrigated Area in the Middle Reaches of the Heihe River in Northwestern China, IEEE Geosci. Remote Sens. Lett., 12, 369-373, 2015.

Ran, Y., Li, X., Sun, R., Kljun, N., Zhang, L., Wang, X., and Zhu, G.: Spatial representativeness and uncertainty of eddy covariance carbon flux measurements for upscaling net ecosystem productivity to the grid scale, Agric. For. Meteorol., 230, 114-127, 2016.

Schmid, H. P.: Footprint modeling for vegetation atmosphere exchange studies: a review and perspective, Agric. For. Meteorol., 113, 159-183, 2002.

Sellers, P., Hall, F., Asrar, G., Strebel, D., and Murphy, R.: The first ISLSCP field experiment (FIFE), Bulletin of the American Meteorological Society, 69, 22-27, 1988.

Sellers, P., Hall, F., Ranson, K. J., Margolis, H., Kelly, B., Baldocchi, D., den Hartog, G., Cihlar, J., Ryan, M. G., and Goodison, B.: The boreal ecosystem-atmosphere study (BOREAS): an overview and early results from the 1994 field year, Bulletin of the American Meteorological Society, 76, 1549-1577, 1995.

Wang, J.: Land surface process experiments and interaction study in China: From HEIFE to IMGRASS and GAME-Tibet/TIPEX, Plateau Meteorol, 18, 280-294, 1999.

Wang, J., Gao, F., and Liu, S.: Remote sensing retrieval of evapotranspiration over the scale of drainage basin, Remote Sensing Technology and Application, 18, 332-338, 2003.

Wang, J., Zhuang, J., Wang, W., Liu, S., and Xu, Z.: Assessment of Uncertainties in Eddy Covariance Flux Measurement Based on Intensive Flux Matrix of HiWATER-MUSOEXE, IEEE Geoscience and Remote Sensing Letters, 12, 259-263, 2015.

Xu, Z., Liu, S., Li, X., Shi, S., Wang, J., Zhu, Z., Xu, T., Wang, W., and Ma, M.: Intercomparison of surface energy flux measurement systems used during the HiWATER-MUSOEXE, Journal of Geophysical Research: Atmospheres, 118, 13140-13157, 2013.

Xu, Z., Ma, Y., Liu, S., Shi, W., and Wang, J.: Assessment of the Energy balance closure under advective conditions and its impact using remote sensing data, Journal of Applied Meteorology and Climatology, 56, 127-140, 2017.

Table 1 Details of the eddy covariance systems in the HiWATER flux matrix

Site No.	Longitude (°)	Latitude (°)	Elevation (m)	Turbulence sensors	Sensor height (m)	Surface type
1	100.3582	38.8932	1552.75	Gill/Li7500A	3.8	Vegetables
2	100.35406	38.88695	1559.09	CSAT3/Li7500	3.7	Maize
3	100.37634	38.89053	1543.05	Gill/Li7500A	3.8	Maize
4	100.35753	38.87752	1561.87	CSAT3/Li7500A	4.2/ 6.2 after 19 Aug.	Residential area
5	100.35068	38.87574	1567.65	CSAT3/Li7500	3.0	Maize
6	100.3597	38.87116	1562.97	CSAT3/Li7500A	4.6	Maize
7	100.36521	38.87676	1556.39	CSAT3/Li7500A	3.8	Maize
8	100.37649	38.87254	1550.06	CSAT3/Li7500	3.2	Maize
9	100.38546	38.87239	1543.34	Gill/Li7500A	3.9	Maize
10	100.39572	38.87567	1534.73	CSAT3/Li7500	4.8	Maize
11	100.34197	38.86991	1575.65	CSAT3/Li7500	3.5	Maize
12	100.36631	38.86515	1559.25	CSAT3/Li7500	3.5	Maize
13	100.37841	38.86076	1550.73	CSAT3/Li7500A	5.0	Maize
14	100.3531	38.85867	1570.23	CSAT3/Li7500	4.6	Maize
15	100.37223	38.85555	1556.06	CSAT3/Li7500A	4.5/ 34	Maize
16	100.36411	38.84931	1564.31	Gill/Li7500	4.9	Maize
17	100.36972	38.8451	1559.63	CSAT3/EC150	7.0	Orchard

Table 2 Details of the Large Aperture Scintillometers in the HiWATER flux matrix

Site	Longitude (°)	Latitude (°)	LAS type, Manufactures	Path length(m)	Effective height (m)
LAS 1	North 100.35090	38.88413	BLS900, Scintec, Germany	3256	33.45
	South 100.35285	38.85470	RR9340, Rainroot, China	3256	33.45
LAS 2	North 100.36236	38.88256	BLS900, Scintec, Germany	2841	33.45
	South 100.36171	38.85717	BLS450, Scintec, Germany	2841	33.45
LAS 3	North 100.37319	38.88338	BLS900, Scintec, Germany	3111	33.45
	South 100.37223	38.85555	LAS, Kipp&zonen, Netherland	3111	33.45
LAS 4	North 100.37841	38.86076	BLS450, Scintec, Germany	1854	22.45
	South 100.36840	38.84682	RR9340, Rainroot, China	1854	22.45

Table 3 Different statistics between LAS observed flux and EC aggregated flux at LAS sites

LAS sites	RMSE [W m^{-2}]	MBE [W m^{-2}]	MAPE [%]
LAS1	0.96	4.25	9.93
LAS2	6.91	2.31	16.39
LAS3	17.63	-18.01	31.70
LAS4	12.75	10.66	33.70

Remarks: $RMSE=\sqrt{\sum_{i=1}^{n}(P_i-O_i)^2/n}$, $MAPE=\frac{100}{n}\sum_{i=1}^{n}\frac{|P_i-O_i|}{\overline{O}}$, $MBE=\sum_{i=1}^{n}(P_i-O_i)/n$, P_i is EC aggregated value，O_i is LAS observed value，$\overline{O}$ is the

mean measured value, n is the number of samples. RMSE is root mean square error, MAPE is mean absolute percentage error, MBE is the

mean bias error.

Table 4 ET for each land cover classes and their proportion of the kernel experimental area ET

Land cover class	Area [km^2]	2012/06/29		2012/06/30	
		ET [m^3 d^{-1}]	ET proportion of total ET [%]	ET [m^3 d^{-1}]	ET proportion of total ET [%]
Maize	17.42	138434.21	81.61	127241.13	83.20
Woods	1.96	12775.93	7.53	12587.64	8.23
Vegetables	1.20	8275.22	4.88	7484.52	4.89
Non-vegetation	3.62	10141.41	5.98	5635.12	3.68
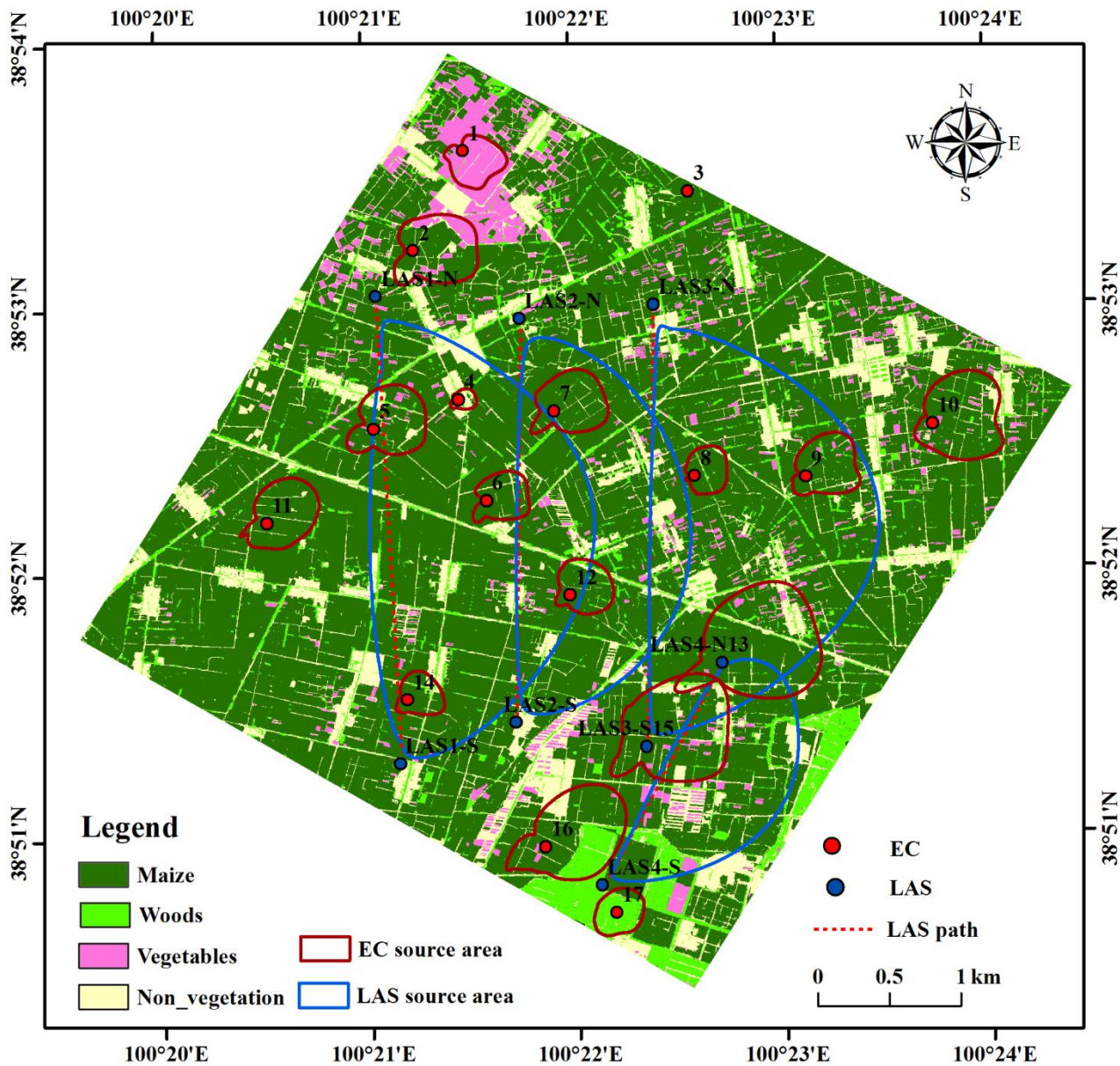
Fig. 1 The land cover map of the kernel experiment area of HiWATER 2012. The small red circles represent the 90 % flux contribution source area of EC sites, and the large blue circles covering different land cover classes indicate the source area of LAS sites on 29 June 2012

27
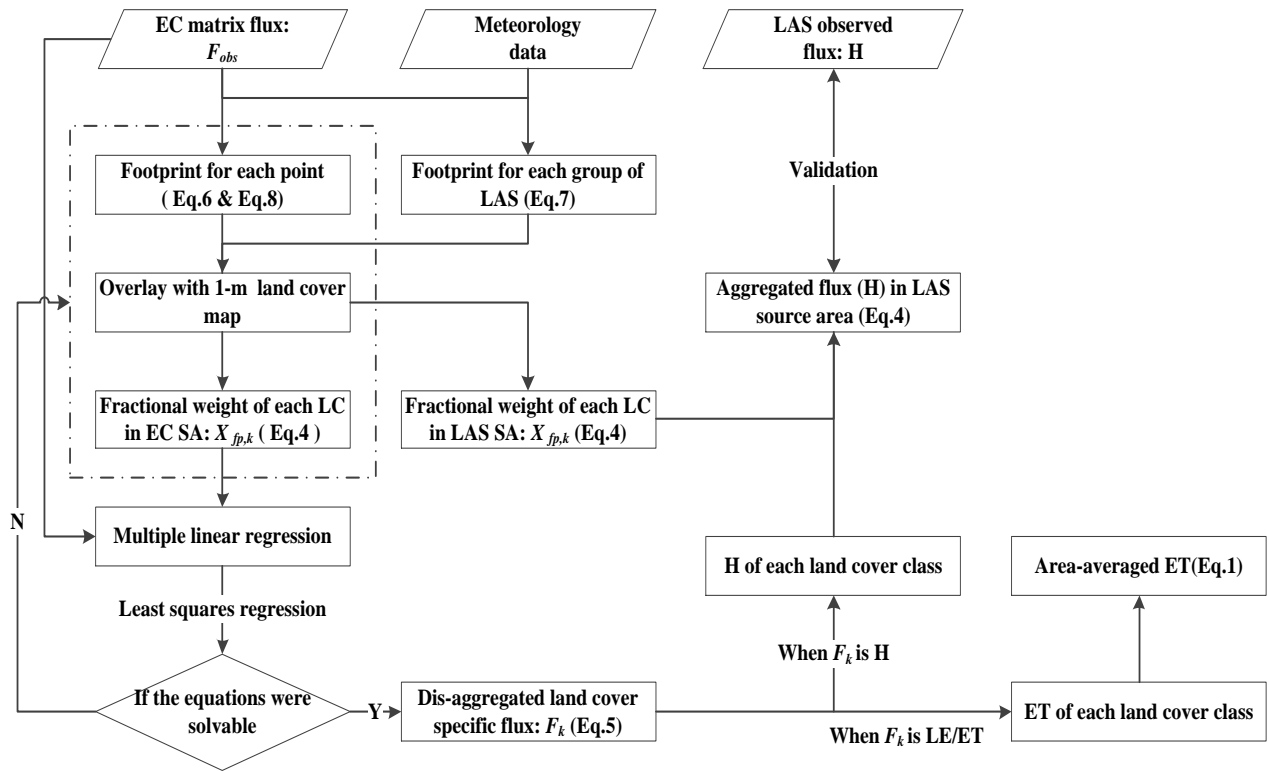
Fig. 2 Schematic illustration of processing steps; LC = land cover class; SA = source area; H = sensible heat flux; LE = latent heat flux; ET = evapotranspiration
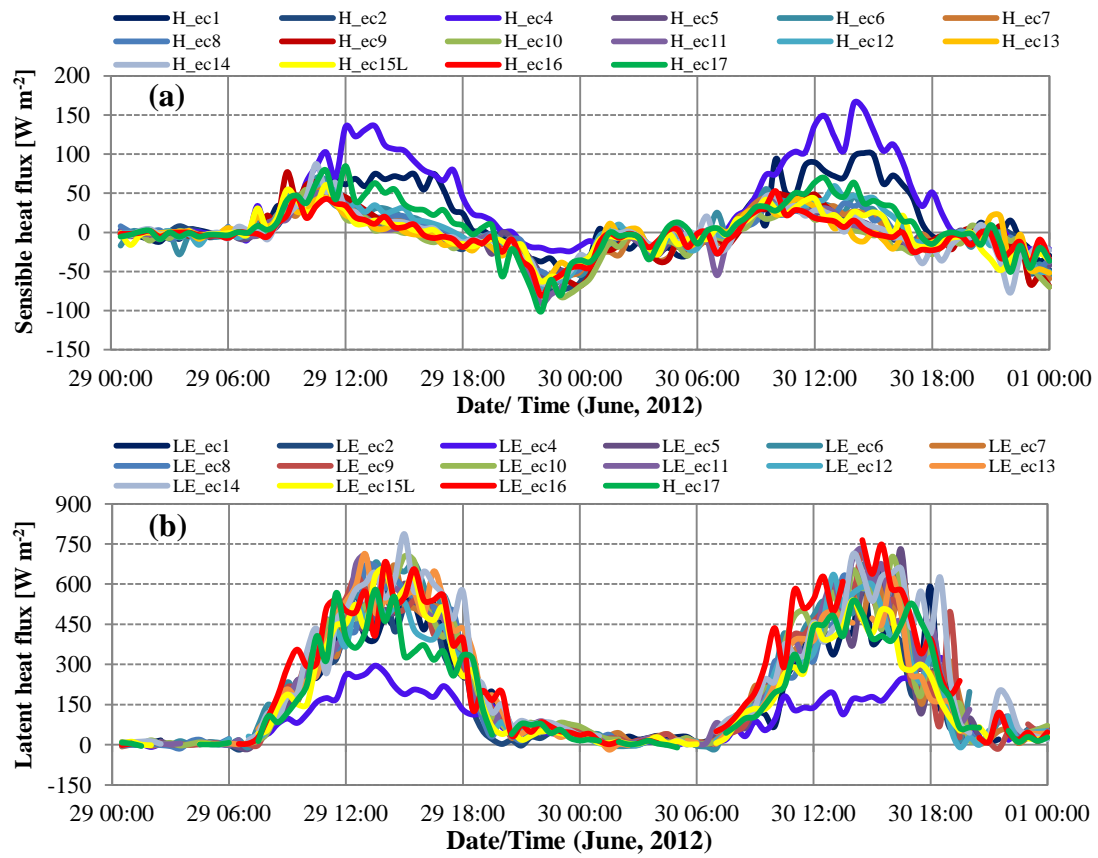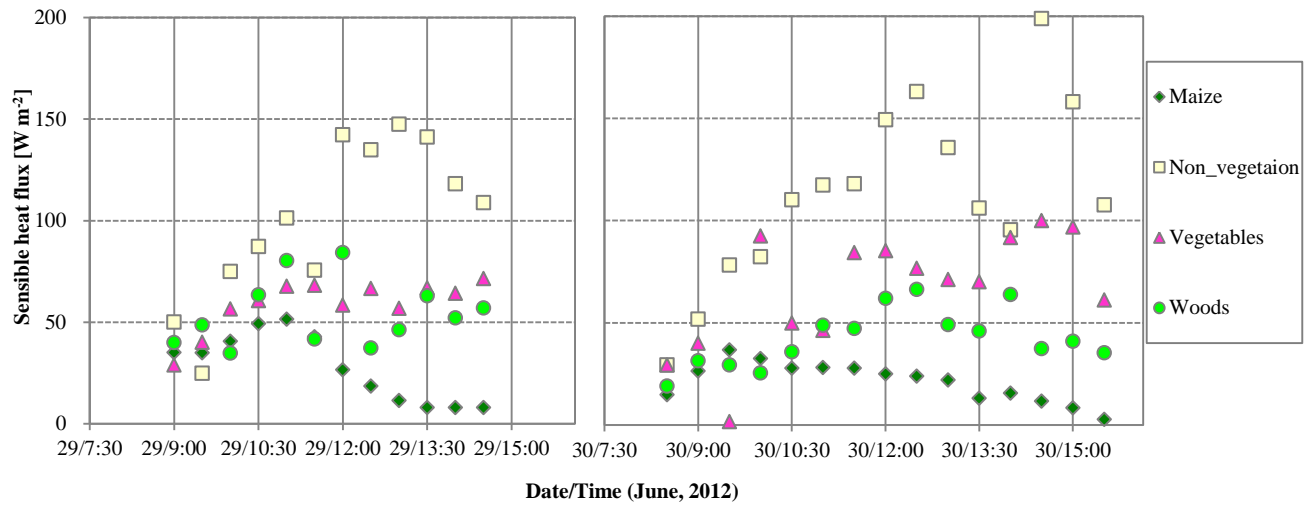
Fig. 3 Diurnal cycle of the sensible heat fluxes (a) and latent heat fluxes (b) between different sites on 29 and 30 June 2012
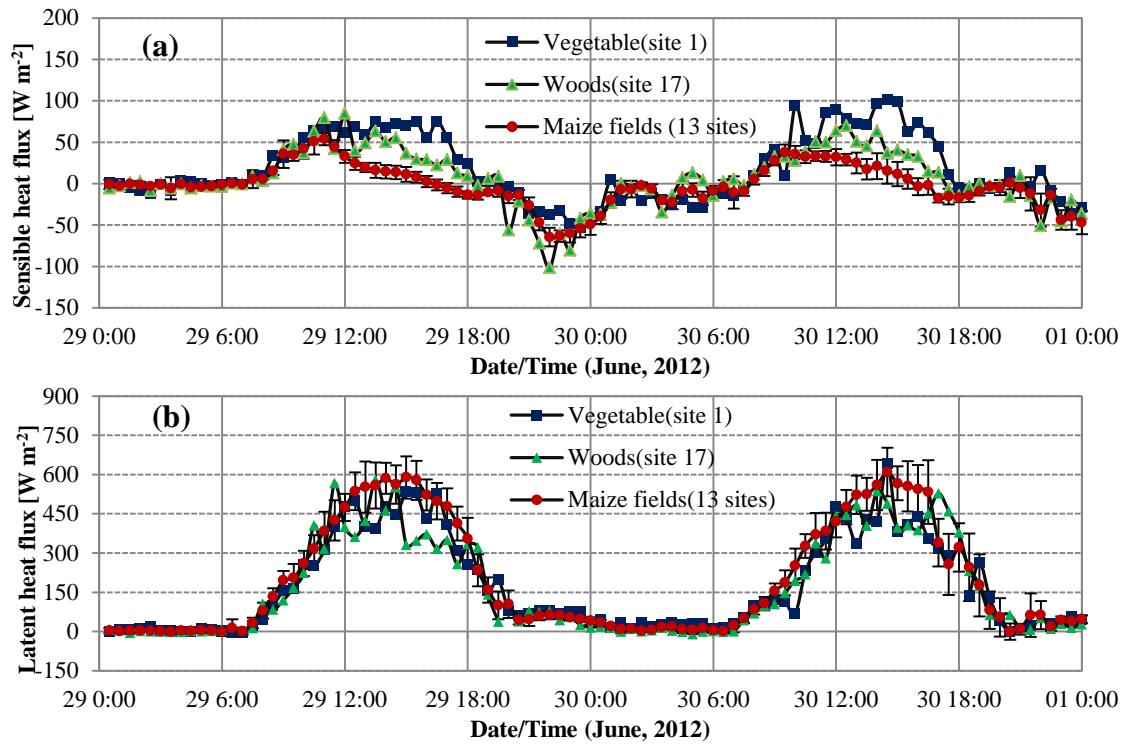
Fig. 4 Diurnal cycle of the mean sensible (a) and latent (b) heat fluxes for 13 maize field sites and different types of vegetation, the errors bars are the standard deviation
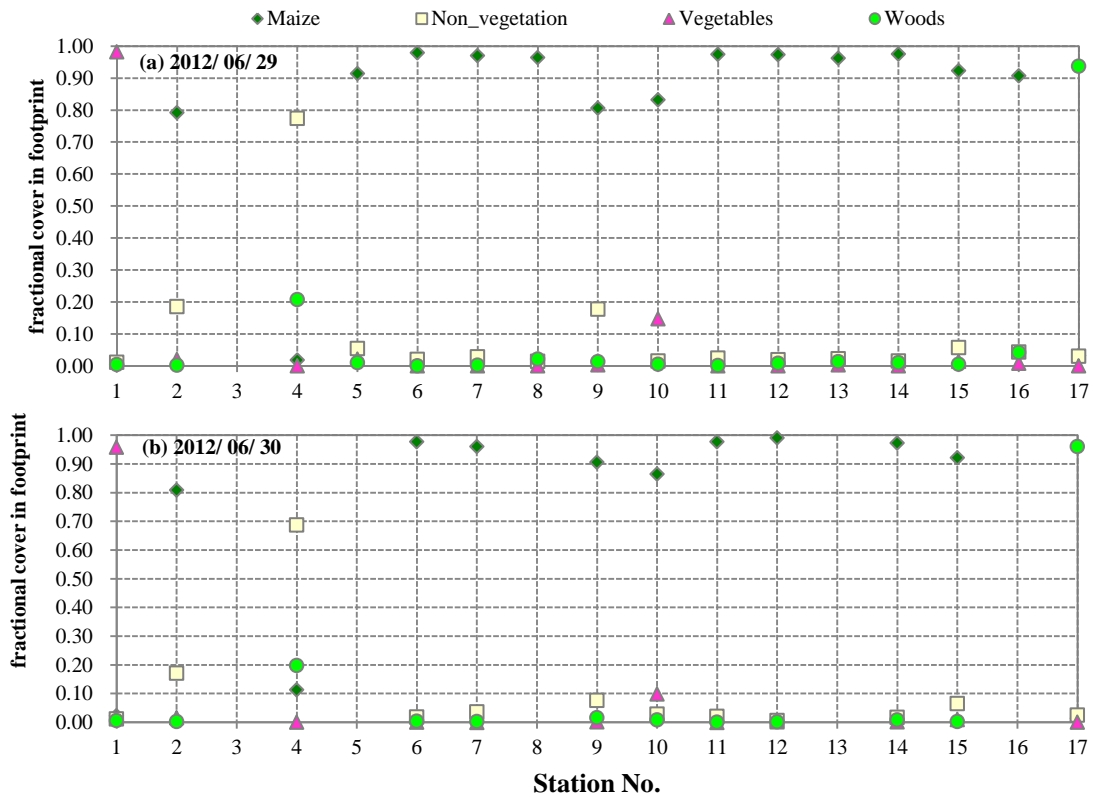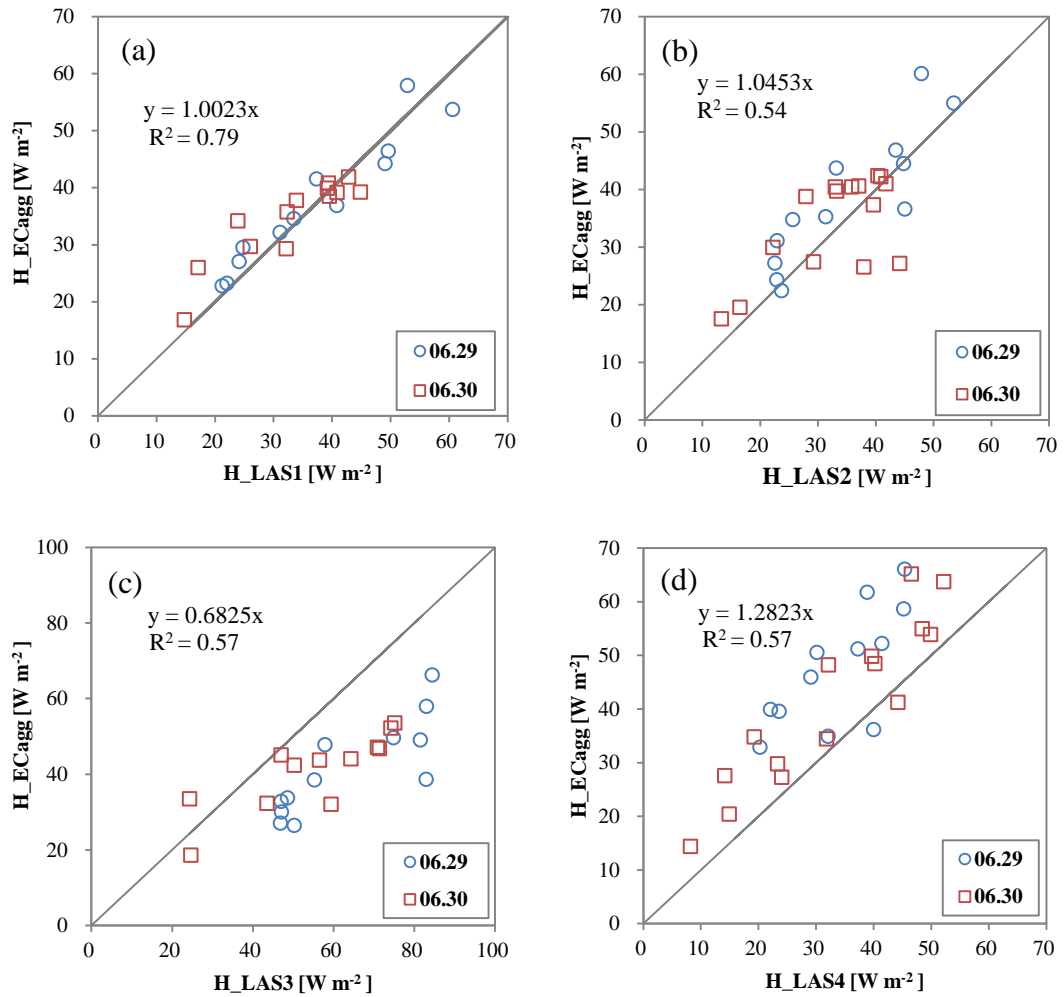
Fig. 5 The fractional weight of each land cover classes in the daily averaged flux footprint of each EC flux measurements on 29 and 30 June 2012
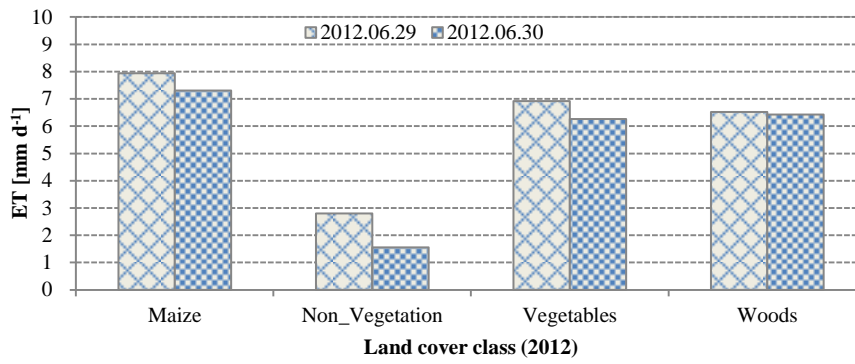
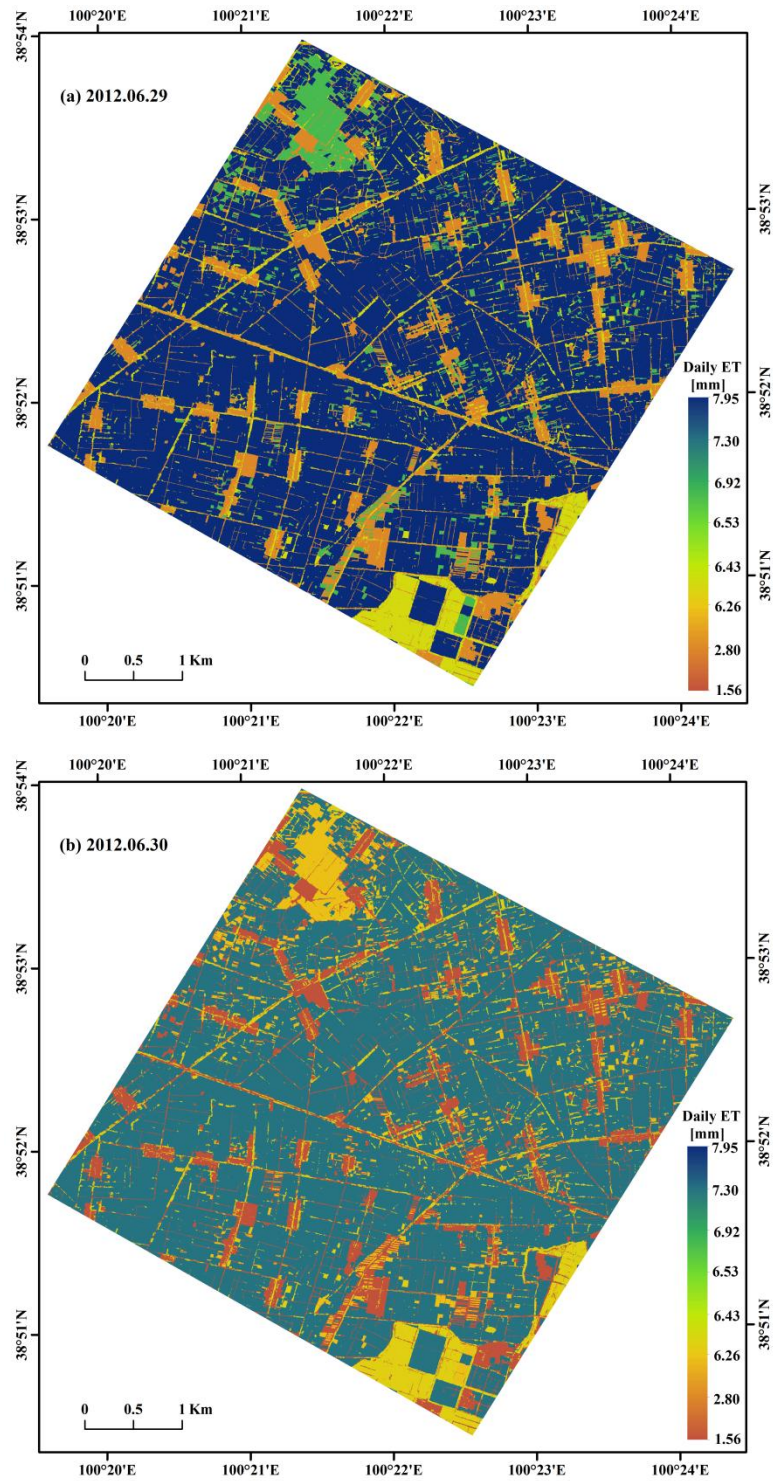**Fig. 6** The diurnal cycle of the sensible heat flux for each land cover classes on 29 and 30 June 2012

Fig. 7 The comparison between LAS observed fluxes (X axis) and EC aggregated fluxes (Y axis)

Fig. 8 The dis-aggregated daily ET of each land covers in the kernel experimental area of HiWATER on 29 and 30 June 2012

Fig. 9 Spatial distribution of averaged daily ET in the kernel experimental area of HiWATER